

# ChemComm

Accepted Manuscript



This is an *Accepted Manuscript*, which has been through the Royal Society of Chemistry peer review process and has been accepted for publication.

*Accepted Manuscripts* are published online shortly after acceptance, before technical editing, formatting and proof reading. Using this free service, authors can make their results available to the community, in citable form, before we publish the edited article. We will replace this *Accepted Manuscript* with the edited and formatted *Advance Article* as soon as it is available.

You can find more information about *Accepted Manuscripts* in the [Information for Authors](#).

Please note that technical editing may introduce minor changes to the text and/or graphics, which may alter content. The journal's standard [Terms & Conditions](#) and the [Ethical guidelines](#) still apply. In no event shall the Royal Society of Chemistry be held responsible for any errors or omissions in this *Accepted Manuscript* or any consequences arising from the use of any information it contains.

# Influence of key amino acid mutation on active site structure and on folding in Acetyl-CoA synthase: a theoretical perspective<sup>†</sup>

Claudio Greco,<sup>\*a</sup> Antonella Ciancetta,<sup>b</sup> Maurizio Bruschi,<sup>a</sup> Alexander Kulesza,<sup>a</sup> Giorgio Moro,<sup>c</sup> and Ugo Cosentino<sup>\*a</sup>

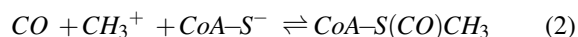
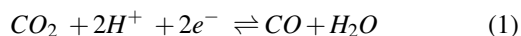
Received Xth XXXXXXXXXXXX 20XX, Accepted Xth XXXXXXXXXXXX 20XX

First published on the web Xth XXXXXXXXXXXX 200X

DOI: 10.1039/b000000x

**Ad hoc quantum chemical modeling of Acetyl-CoA synthase local structure and folding allowed us to identify an unprecedented coordination mode of histidine sidechain to protein-embedded metal ions.**

Acetyl-CoA synthase/Carbon monoxide dehydrogenase (ACS/CODH) is a bifunctional enzyme that is able to catalyze two different reactions:



Reactions 1 and 2 are catalyzed by the CODH and ACS portions of the enzyme, respectively. Apart from the obvious enzymological interest, the study of ACS/CODH system might inspire the development of biomimetic catalysts for the abatement of environmental CO and CO<sub>2</sub>.<sup>1</sup>

As far as reaction 1 is concerned, the C-cluster – a cofactor including Ni and Fe ions<sup>1,2</sup> – processes CO<sub>2</sub> within the enzyme; the CO thus produced is transferred through a gas channel<sup>3,4</sup> to another metal-containing active site, which catalyzes reaction 2. The latter is termed A-cluster, and is composed of two subsites: a Fe<sub>4</sub>S<sub>4</sub> cubane and a peculiar dinickel moiety, bridged to each other by a cysteinyl sulphur ligand (Cys509 in the sequence of the enzyme from *Moorella thermoacetica*, which is considered hereafter). Based on their position with respect to the cubane, the Ni ions are termed proximal (Ni<sub>p</sub>) or distal (Ni<sub>d</sub>), see Fig. 1. The Ni-containing subsite binds and processes the substrates CO and CoA-S<sup>-</sup>, and several theoretical studies employing density functional theory (DFT) were

carried out to unveil its mechanism of action.<sup>5–9</sup> One of the most recent investigations – published by Field *et al.*<sup>8</sup> – was based on explicit inclusion of both the Fe<sub>4</sub>S<sub>4</sub> and the dinickel subsites in the DFT representation of the A-cluster. This allowed to show that binding of CO to Ni<sub>p</sub> in its monovalent state, followed by attack of methyl cation at the same site, would be accompanied by transfer of one electron from the Fe<sub>4</sub>S<sub>4</sub> site to the dinickel site. Subsequent formation of the C–C bond between the carbon atoms of the two substrates would precede the detachment of the acetyl ligand, with concomitant formation of acetyl-CoA from coenzyme A.<sup>8</sup>

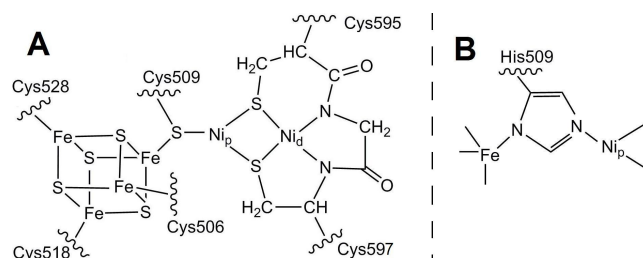


**Fig. 1** A: wild type A-cluster; B: C509H mutant version, with the hypothetical disposition of the histidinate as proposed in ref.<sup>10</sup>

Clearly, the catalytic cycle above mentioned foresees a redox role for the Fe<sub>4</sub>S<sub>4</sub> subsite, whereas previous experimental evidences are against the possibility of redox changes in the iron-sulfur cubane during turnover.<sup>11</sup> A biochemical approach to better understand the role of the components of the A-cluster is the one based on the introduction of mutation(s) affecting the amino acids directly bound to the metal ions. In such context, Tan *et al.* recently<sup>10</sup> introduced mutations at the level of bridging Cys509 residue: mutations at this site are expected to modify the relative redox potentials of the metal subsites as well as the electronic communication between them. In particular, it was found that replacement of cysteine with histidine (C509H mutation hereafter) allows to retain 70% of the enzymatic activity of the wild-type enzyme: a surprising result given very rare occurrence of histidines bound to Fe<sub>4</sub>S<sub>4</sub> clusters, and given the fact that histidine sidechain is

<sup>†</sup> Electronic Supplementary Information (ESI) available: Methodological details, preliminary bioinformatics analysis, selected DFT-optimized geometries, results of natural bond orbital analyses. See DOI: 10.1039/b000000x/

<sup>a</sup> Department of Earth and Environmental Sciences, Milano-Bicocca University, P.zza della Scienza 1, 20126, Milan, Italy Tel: +39-02-6448-2098/2822; E-mail: claudio.greco@unimib.it, ugo.cosentino@unimib.it

<sup>b</sup> Department of Pharmaceutical and Pharmacological Sciences, University of Padova, Via Marzolo 5, 35131 Padova, Italy.

<sup>c</sup> Department of Biotechnologies and Biosciences, Milano-Bicocca University, P.zza della Scienza 2, 20126, Milan, Italy

much bulkier than the one of cysteine. The authors speculated that the imidazole ring is able to functionally replace a thiolate by inserting between the  $\text{Fe}_4\text{S}_4$  and dinickel subclusters.<sup>10</sup> In practice, this would correspond to having the His509 in its fully deprotonated, histidinate form, with one of the imidazole N atoms bound to the  $\text{Ni}_p$  center, and the other one coordinated to one of the Fe atoms of the cubane (Fig 1B). However, no conclusive information on such key structural issue has been published yet, while it is obvious that a final answer on the structural features of the A-cluster in the C509H mutant has to be provided, in order to gain a clear picture on the implications contained in the experimental results.<sup>10</sup>

In view of this, we evaluated the possible effects of the presence of a bridging histidinate on the A-cluster structure by exploratory DFT optimizations. That is, we performed qualitative calculations on models of the wild type or mutant A-cluster, without explicit representation of the surrounding protein matrix; such models ( $^{wt}\mathbf{a}$  and  $^{mut}\mathbf{a}$ , optimized structures shown in ESI) only included the atoms composing the  $\text{Fe}_4\text{S}_4$  and dinickel subclusters, in analogy with the approach followed in the above mentioned study by Field *et al.*. Energy minimization of  $^{wt}\mathbf{a}$  and  $^{mut}\mathbf{a}$  – carried out using either pure (BP86)<sup>12,13</sup> or hybrid (B3LYP)<sup>14,15</sup> density functionals and applying the broken symmetry (BS) approach<sup>16–18</sup> to treat antiferromagnetic coupling at the  $\text{Fe}_4\text{S}_4$  site – demonstrated that major structural reorganization of the protein active site would be needed to accommodate a bridging histidinate, due to its bulkiness. In fact, the mutant A-cluster model elongates by more than 3 Å with respect to the wild-type (Fig. S3, S4 in ESI).

Further, to gain a more detailed picture of the structure of the mutant, we developed an *ad hoc* large-size fully DFT model of the active site and surroundings, a challenging task; in fact, it was needed to take into account the essential structural features of the enzyme, including the steric constraints imposed by the protein matrix that harbors the A-cluster. To this end, we exploited the fact that the portion of apoprotein in proximity of the A-cluster is structurally conserved (see ESI for details; see also previous experimental studies by Tan *et al.*<sup>19</sup> on the stability of relevant protein fragments), and is included in a continuous stretch of protein sequence between amino acids 503 and 599. In this regard, the blue portion of the protein in Fig. 2A represents the backbone region directly involved in coordination of all Fe and Ni ions. Notably, the subregion 537–572 is poor of  $\alpha$  helices and  $\beta$  strands (see the protein portion coloured in cyan in Fig. 2B); as it is only partially structured, it is reasonable to assume that it does not exert a large effect on the flexibility of the flanking, more structured regions. In view of this, we neglected the 537–572 subregion in our model; moreover, we mutated to glycines all the residues whose sidechains point away from protein portions that are explicitly represented in the model itself (details

in ESI). These modifications led to the  $\sim 700$  atoms system shown in Fig. 2C. This model was then treated using the BP86 functional, the TZVP basis for the A-cluster atoms, whereas the SV basis<sup>20</sup> was used for the surrounding protein matrix (see ESI for details); if not stated otherwise, the BS scheme adopted hereafter – termed *BSI* – is the one obtained after convergence of the first self-consistent field (SCF) calculation on the model featuring wild-type A-cluster (see  $^{wt}\mathbf{A1}_{\text{Cys}^-}$  in Fig. 2, and the inset therein) while the fully oxidized state of the latter was considered in order to assign the overall charge to the systems (see ESI).

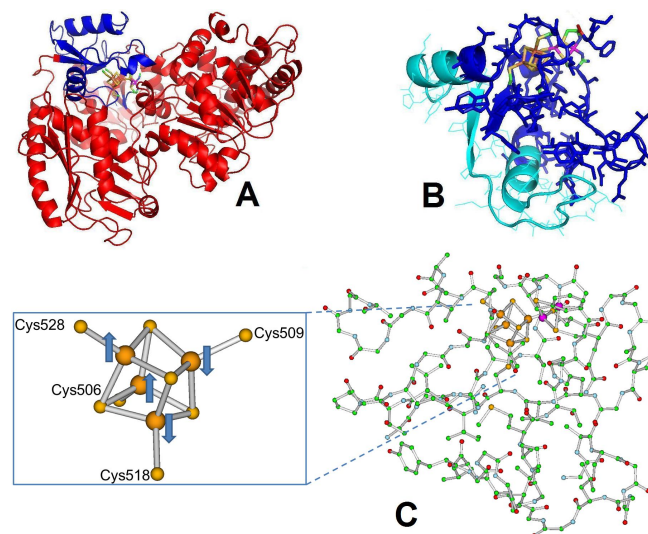


**Fig. 2** A: the ACS subunit of the ACS/CODH enzyme; B: the sequence portion between aminoacids 503–599, with the subregion 537–572 highlighted in cyan; C: the DFT-optimized geometry of  $^{wt}\mathbf{A1}_{\text{Cys}^-}$  (H atoms not shown; C, N, O, S, Fe, Ni atoms colored in green, blue, red, yellow, brown and violet, respectively). In the inset, it is shown the BS scheme on which the SCF calculation converged, before the A-cluster was allowed to relax from crystallographic geometry. This spin-coupling scheme will be referred to as “*BSI*”

As a first step, we considered the wild-type ACS ( $^{wt}\mathbf{A1}_{\text{Cys}^-}$ , Fig. 2C): in order to verify whether the model is able to reproduce the local structural features of the enzyme, full geometry optimization of  $^{wt}\mathbf{A1}_{\text{Cys}^-}$  was carried out and root mean square deviation (RMSD) of positions of backbone atoms with respect to the corresponding crystallographic data was computed. Notably, such RMSD turned out to be as low as 0.76 Å. This small value confirms that our large size model is able to reproduce the local features of the protein architecture, as well as the steric constraints imposed by the protein matrix on the active site. It is important to stress that such result is obtained *without* the imposition of arbitrary constraints on atomic positions, which are typically introduced in the “quantum chemical cluster approach” applied in many theoretical

bioinorganic studies.<sup>21</sup>

Geometry optimization of the mutant, starting from a conformation featuring the previously proposed connectivity (see ref.<sup>10</sup> and Fig. 1) leads to the detachment of one of the N atoms of the imidazole ring from the  $\text{Ni}_p$  atom. The resulting A-cluster structure is reported in Fig. 3 (model  $\text{mut A2}_{\text{His}^-}$ ). In this conformation, an unusual interaction between the  $\pi$  system of the imidazole ring and  $\text{Ni}_p$  is established, a kind of bonding which has been previously described in synthetic complexes,<sup>22</sup> but that has no counterparts in X-ray structures within the Protein Data Bank.<sup>23</sup> Optimization of a small-size model which includes the A-cluster atoms only and neglects explicit treatment of the surrounding protein matrix (see ESI for details) indicates that the active site conformation observed in  $\text{mut A2}_{\text{His}^-}$  is strained: the energy gap computed at BP86/TZVP between such relaxed A-cluster model and the parent structure is 14.1 kcal/mol. Notably, within the accuracy of DFT the latter result is substantially confirmed by single point B3LYP/TZVP calculations at the BP86 geometry, which provide a 3.9 kcal/mol larger estimate of strain. As for the characterization of the electronic structure of the A-cluster mutant, the above mentioned Ni- $\pi$  system interaction was confirmed by natural bond orbital (NBO) analysis, which evidenced relevant donation of electron density from the imidazole ring to the metal (see ESI). We also evaluated the effects of a change in the BS coupling at the  $\text{Fe}_4\text{S}_4$  site, both in terms of variation of total energy in the large-size mutant model, and in terms of consequences on histidine coordination mode. To this end,  $\text{mut A2}_{\text{His}^-}$  was reoptimized after imposing one of the two spin-coupling schemes *BS2* and *BS3* schematically shown in Fig. 4, alternative with respect to the *BS1* scheme (see Fig. 2). In line with previous theoretical results on a metalloenzyme system bearing Fe/S clusters,<sup>18</sup> it turned out that total energy varies significantly as a function of the BS coupling adopted, with *BS2* and *BS3* lying lower in energy than *BS1* by 14.7 and 9.6 kcal/mol, respectively. However, key structural parameters of the model remain essentially unaltered: the interatomic distances highlighted in Fig. 3 for  $\text{mut A2}_{\text{His}^-}$  undergo maximum deviation of 0.04 Å following change in BS coupling scheme.

To deepen further insights into the potential effects of His residue bulkiness on protein and active site conformation, we also performed a geometry optimization of our large-size mutant model, in which the starting structure presented a significant displacement of the backbone region including the  $\text{Ni}_d$ -coordinated N atoms. The latter DFT calculation led to a final geometry in which the histidinate is metal-coordinated at both N atoms of the ring (see  $\text{mut A3}_{\text{His}^-}$ , Fig. 3). For a judgement of possible consequences of this mutation on protein stability, we analysed the surrounding of the A-cluster. This analysis focused on residue Phe598 which in the amino acid sequence follows the  $\text{Ni}_d$ -coordinated Cys597, and is located at the be-

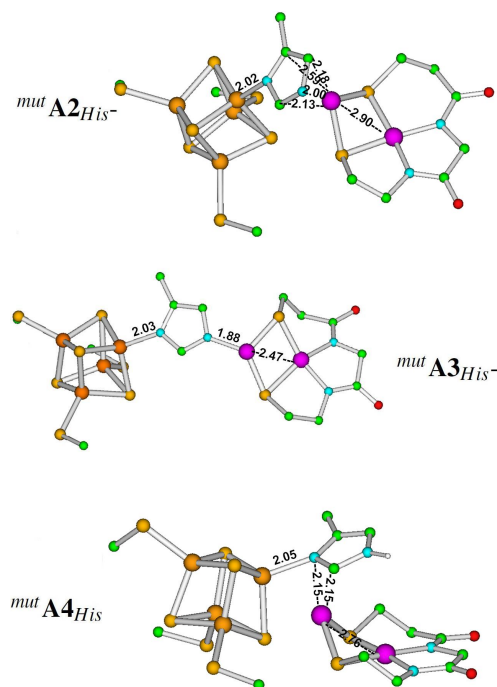


**Fig. 3** Geometry of A-cluster in  $\text{mut A2}_{\text{His}^-}$ ,  $\text{mut A3}_{\text{His}^-}$ ,  $\text{mut A4}_{\text{His}}$ . All interatomic distances in Å. Colour code as in Fig. 2

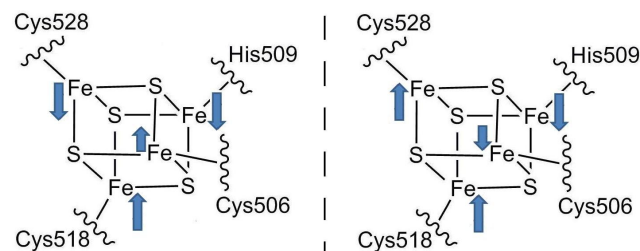


**Fig. 4** BS schemes denoted *BS2* (on the left) and *BS3*

ginning of a  $\beta$  strand deeply buried in the protein matrix (Fig. S7 in ESI). The backbone atoms of this residue are displaced by around 5 Å from the crystallographic position, and undergo large changes in spatial orientation. This would favour misfolding of the protein, a picture which is difficult to reconcile with the experimentally observed retention of activity and stability in the mutant.

As a next step, we reoptimized model  $\text{mut A2}_{\text{His}^-}$ , after addition of one proton to the  $\text{N}^{\epsilon 2}$  atom. The geometry obtained is reported in Fig. 3 ( $\text{mut A4}_{\text{His}}$ ). It features the unprotonated N atom of the imidazole ring in bridging position between the dinickel and the  $\text{Fe}_4\text{S}_4$  sites. More specifically, one of the iron atoms in the cubane is bound only to the  $\text{N}^{\delta 1}$  atom, whilst the  $\text{Ni}_p$  is at short distance from both the latter nitrogen and the adjacent  $\text{C}^{\epsilon 1}$  atoms of the imidazole ring. This points again

at an interaction between  $\text{Ni}_p$  and the histidine  $\pi$  system, as also confirmed by NBO analysis, which evidenced prominent backdonation from  $\text{Ni}_p$  to the imidazole ring (see ESI).

Finally, we also considered the two-electron reduced form of  $^{\text{mut}}\text{A4}_{\text{His}}$  as a model of the enzyme state which forms upon activation of the oxidized ACS enzyme. In fact, the redox states of metal centers within the wild-type A-cluster following reductive activation is matter of current debate, with alternative possibilities supported by different sets of experimental and theoretical data.<sup>8,24,25</sup> Optimization of  $^{\text{mut}}\text{A4-red}_{\text{His}}$  – see Fig. 5 for the A-cluster geometry within the model – were followed by population analyses carried out as described in details in ESI. The latter evidenced that the  $\text{Fe}_4\text{S}_4(\text{Cys})_3(\text{His})$  fragment has an overall charge of  $-1.82 e$ , indicating that the cubane attains the reduced,  $3\text{Fe(II)Fe(III)}$  state in the model. As for the dinickel site, it turned out that the charge of the  $\text{Ni}_2(\text{RNR}')(\text{R}''\text{NR}''')(\mu\text{-Cys})_2$  bisamidate/bisthiolate fragment is  $-1.18 e$ , a result compatible with a mixed-valence  $\text{Ni(I)Ni(II)}$  state. Notably, atomic spin population of  $\text{Ni}_d$  is zero, whereas the one of  $\text{Ni}_p$  is 0.90: this indicates that the site which attains the monovalent state is the latter. In ESI, we also describe population analyses on the two-electron reduced form of  $^{\text{mut}}\text{A2}_{\text{His}}$ , termed  $^{\text{mut}}\text{A2-red}_{\text{His}}$ : the results obtained for the latter are analogous to the ones reported in the lines above for  $^{\text{mut}}\text{A4-red}_{\text{His}}$ .

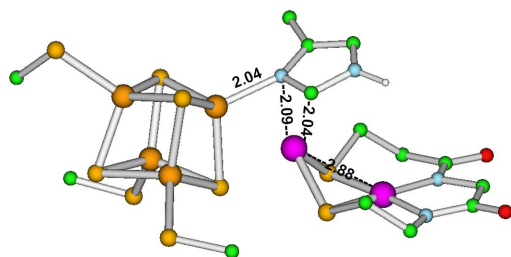


**Fig. 5** Geometry of A-cluster in  $^{\text{mut}}\text{A4-red}_{\text{His}}$ . All interatomic distances in Å. Colour code as in Fig. 2

In conclusion, we applied an unprecedented, fully quantum-mechanical approach beyond the standard "cluster modeling" to judge effects of mutation on protein folding. After validating our large-size model including the A-cluster in fully oxidized state and its surroundings, we performed geometry optimization of a mutant, in which a key cysteine residue of the active site is replaced with histidine. This allowed us to demonstrate that the presence of a bridging histidinate as represented in Fig. 1B would require substantial changes in the fold of the protein, which are unlikely as they would contradict the experimentally observed retention of catalytic activity upon mutation. The alternative picture provided by our DFT model foresees a configuration where the  $\text{Ni}_p$  atom interacts with the  $\pi$  system of the histidine - independently of protonation state of the imidazole ring - thereby minimizing

the mutation-induced stress. The effects of two-electron reduction of the model were also matter of investigation; future studies will focus on the characterization of other possible intermediates within the enzyme catalytic cycle, in order to dissect the consequences of Cys509 mutation on the mechanism of acetyl-CoA synthesis.

This work was supported by the Cluster of Excellence for Catalysis UniCat (Berlin, Germany) and by the University of Milano-Bicocca (FA2012-2013). The authors wish to thank Prof. R. Della Pergola for valuable discussions.

## References

- 1 Y. Kung, T. I. Doukov, J. Seravalli, S. W. Ragsdale and C. L. Drennan, *Biochemistry*, 2009, **48**, 7432.
- 2 C. Darnault, A. Volbeda, E. J. Kim, P. Legrand, X. Vernede, P. A. Lindahl and J. C. Fontecilla-Camps, *Nat. Struct. Biol.*, 2003, **10**, 271.
- 3 E. L. Maynard and P. A. Lindahl, *J. Am. Chem. Soc.*, 1999, **121**, 9221.
- 4 J. Seravalli and S. W. Ragsdale, *Biochemistry*, 2000, **39**, 1274.
- 5 R. P. Schenker and T. C. Brunold, *J. Am. Chem. Soc.*, 2003, **125**, 13962.
- 6 J. L. Craft, B. S. Mandimutsira, K. Fujita, C. G. Riordan and T. C. Brunold, *Inorg. Chem.*, 2003, **42**, 859.
- 7 C. E. Webster, M. Y. Darensbourg, P. A. Lindahl and M. B. Hall, *J. Am. Chem. Soc.*, 2004, **126**, 3410.
- 8 P. Amara, A. Volbeda, J. C. Fontecilla-Camps and M. J. Field, *J. Am. Chem. Soc.*, 2005, **127**, 2776.
- 9 A. Chmielowska, P. Lodowski and M. Jaworska, *J. Phys. Chem. A*, 2013, **117**, 12484.
- 10 Y. Liu, X. Zhu, F. Wang, T. Ying, P. Li, Z.-X. Huang and X. Tan, *Chem. Commun.*, 2011, **12**, 1417.
- 11 X. Tan, C. Sewell, Q. Yang and P. A. Lindahl, *J. Am. Chem. Soc.*, 2003, **125**, 318.
- 12 A. D. Becke, *Phys. Rev. A*, 1988, **38**, 3098.
- 13 J. Perdew, *Phys. Rev. B*, 1986, **33**, 8822.
- 14 A. D. Becke, *J. Chem. Phys.*, 1993, **98**, 5648.
- 15 C. T. Lee, W. T. Yang and R. G. Parr, *Phys. Rev. B*, 1988, **37**, 785.
- 16 L. Noodleman and J. G. Norman, *J. Chem. Phys.*, 1979, **70**, 4903.
- 17 L. Noodleman, *J. Chem. Phys.*, 1981, **74**, 5737.
- 18 C. Greco, P. Fantucci, U. Ryde and L. De Gioia, *Int. J. Quantum. Chem.*, 2011, **111**, 3949.
- 19 Y. Liu, F. Wang, P. Li and X. Tan, *ChemBioChem*, 2011, 1291.
- 20 A. Schaefer, H. Horn and R. Ahlrichs, *J. Chem. Phys.*, 1992, **97**, 2571.
- 21 F. Himmo and P. Siegbahn, *WIRE Comput. Mol. Sci.*, 2011, **1**, 323.
- 22 M. Kreye, A. Gloeckner, C. G. Daniliuc, M. Freytag, P. G. Jones, M. Tamm and M. D. Walter, *Dalton Trans.*, 2013, **42**, 2192.
- 23 *In view of this result, we optimized also the second possible rotamer of the H509 residue (see  $^{\text{mut}}\text{A5}_{\text{His}}$  in ESI, Fig. S6). However, this structure is much less stable than the previous one ( $\Delta E = 22.9$  kcal/mol).*
- 24 P. A. Lindahl, *J. Biol. Inorg. Chem.*, 2004, **9**, 516.
- 25 S. W. Ragsdale, *J. Biol. Inorg. Chem.*, 2004, **9**, 511.